Electrical Power and Energy Systems 32 (2010) 656–663

Contents lists available at ScienceDirect

Electrical Power and Energy Systems

journal homepage: www.elsevier.com/locate/ijepes

On the effect of AVR gain on bifurcations of subsynchronous resonance in power systems

Mohammad S. Widyan *

Electrical Engineering Department, The Hashemite University, 13115 Zarqa, Jordan

ARTICLE INFO

Article history:
Received 22 May 2007
Accepted 10 November 2009

Keywords:
Subsynchronous resonance
Power system dynamics
AVR
Bifurcation

ABSTRACT

This paper presents the effect of the automatic voltage regulator (AVR) gain on the bifurcations of subsynchronous resonance (SSR) in power systems. The first system of the IEEE second benchmark model of SSR is chosen for numerical investigations. The dynamics of both axes damper windings of the generator and that of the power system stabilizer (PSS) are included. The bifurcation parameter is the compensation factor. Hopf bifurcation, where a pair of complex conjugate eigenvalues of the linearized model around the operating point transversally crosses from left- to right-half of the complex plane, is detected in all AVR gains. It is shown that the Hopf bifurcation is of subcritical type. The results also show that the location of the Hopf bifurcation point i.e. the stable operating point regions are affected by the value of the AVR gain. The variation of the location of the Hopf bifurcation point as function of the AVR gain for two operating conditions is obtained. Time domain simulation results based on the nonlinear dynamical mathematical model carried out at different compensation factors and AVR gains agree with that of the bifurcation analysis.

1. Introduction

Subsynchronous resonance (SSR) is an electric power condition where the electric network exchanges energy with a turbine generator at one or more of the natural frequencies of the combined system below the synchronous frequency of the system. Basically, there are two aspects of the SSR problem, self-excitation (also called as steady state SSR) and transient torques (also called as transient SSR). The self-excitation is resulted mainly from the subsynchronous frequency currents entering the generator terminals. These currents produce subsynchronous frequency terminal voltage components, which may sustain the currents to produce the effect that is termed as self-excitation. There are two types of self-excitation, one involves only rotor electrical dynamics and the other involves both rotor electrical and mechanical dynamics. The first one is termed as induction generator effect while the second one is called torsional interaction. Transient torques, on the other hand, are resulted from the system disturbances which can excite oscillatory torques on the generator rotor. The transient electrical torque, in general, has many components including unidirectional, exponentially decaying and oscillatory torques from subsynchronous to multiples (typically second harmonic) of network frequency. Due to SSR phenomenon, the subsynchronous frequency components of torque can have large amplitudes immediately following the disturbance, although they may decay eventually. Each occurrence of these high amplitude transient torques can result in expenditure of the shaft life due to fatigue damage [1].

Different approaches in subsynchronous resonance analysis are presented in the literature. Eigenvalue analysis [2–4] and others, frequency scanning method [5–7], time domain simulation [8] and Electromagnetic Transient Program (EMTP). Recently, power system dynamics have been studied from nonlinear dynamics point of view using bifurcation theory. In fact, power system has rich bifurcation phenomena. Particularly, when the consumer demand for reactive power reaches its peak, the dynamics of an electric power network may move to its voltage stability margin leading to oscillations and bifurcations [9,10]. In addition to the constant reactive power, the coefficient of the reactive impedance is used as bifurcation parameter [11]. Saddle node, subcritical and supercritical Hopf, cyclic fold, period doubling bifurcations and chaotic attractors are obtained. Nonlinear controllers were used to control the subcritical and period doubling bifurcations. A comprehensive study of bifurcations in a realistic power system model in which the generator input mechanical power and both active and reactive power demand at the load bus were used as bifurcation parameters [12]. The dynamics of the q-axis damper winding and the dynamics of AVR with V_{ref} as bifurcation parameter were included.

SSR is another power system phenomenon, in addition to the voltage collapse, in which bifurcation theory can be applied. The

* Tel.: +962 5 3903333x5012.
E-mail address: mohammadwidyan@yahoo.com

0142-0615/$ - see front matter © 2009 Elsevier Ltd. All rights reserved.
doi:10.1016/j.ijepes.2009.11.024

most common bifurcation is the dynamic bifurcation "Hopf bifurcation" where a complex conjugate pair of eigenvalues of the linearized model around the operating point transversally crosses from left- to right-half of the complex plan. The birth of a limit cycle from an equilibrium point gives rise to oscillations, which may undergo complicated bifurcations such as period multiplication, cyclic folds or crises. The Hopf bifurcation theorem, in which the dynamics of the AVR and damper windings are neglected, was used to study a Single Machine Infinite Bus (SMIB) power system experiencing SSR [8]. A prediction of supercritical Hopf bifurcation was investigated. The bifurcation analysis was used to investigate the complex dynamics of a heavily loaded SMIB power system modeling the characteristics of the BOARDMAN generator with respect to the rest of the North-Western American Power System [13]. In their study, the dynamics of the *d*- and *q*-axes damper windings were included while that of the AVR was neglected. The results show that as the compensation factor increases the operating point loses stability via supercritical Hopf bifurcation. On further increase of the compensation factor the system route to chaos via torus breakdown. The effect of electrical machine saturation on SSR was also studied [14]. The conclusion was that the generator saturation slightly shrinks the positively damped region by shifting the Hopf bifurcation point to smaller compensation level. It also slightly shifts the secondary Hopf bifurcation and bluesky catastrophe to smaller compensation level.

Bifurcation control deals with modification of bifurcation characteristics of a parameterized nonlinear system by a designed control input. Typical bifurcation control objectives include delaying the appearance of inherent bifurcation [15], stabilizing a bifurcated solution or branch [11], changing the parameter value of an existing bifurcation point [16], introducing a new bifurcation at a preferable parameter value, monitoring the multiplicity, amplitude [17] and/or frequency of some limit cycles emerging from bifurcation, optimizing the system performance near a bifurcation point [18] and a combination of some of these objectives.

There are three distinct types of excitation systems based on the power source of the exciter. (1) DC excitation system, which utilizes a DC generator with commutator. (2) AC excitation system, which uses alternators and either stationary or rotating rectifiers to produce the direct current for the field. (3) Static excitation system in which the power is supplied through transformers and rectifiers. The first two types are also called rotating exciters which are mounted on the same shaft of the generator and prime mover. Power system stabilizers (PSS) which are supplementary controllers in excitation systems has an input signal derived from rotor speed, bus frequency, electrical power or a combination of these variables. The output of the PSS is added to the summing junction at the input of AVR. The main objective of the PSS is to provide additional damping torque. Usually, PSS consists of washout circuit and phase compensator. The objective of the washout circuit is to act as a high pass filter, preventing DC and very low frequency components. The time constants of the phase compensation are selected to provide appropriate phase compensation in the range of frequencies typically from 0 to 3.5 Hz. The effect of the linear and nonlinear controllers on bifurcations of SSR is studied [19]. It is shown that the linear controllers increase the compensation level at which subsynchronous resonance occurs while the nonlinear controller does not affect the location and type of the Hopf bifurcation. It is also shown that the larger the nonlinear controller gain is, the smaller the amplitude of the limit cycle tends to be. The bifurcation theory is applied on the first system of the IEEE second benchmark model of subsynchronous resonance. A nonlinear controller of the form $K(\omega_g^3 - \omega_1^3)$ has been designed where all the bifurcations of the system were eliminated at all realistic compensation factors despite the successive interactions of the subsynchronous electrical mode with the three torsional mechanical modes [20–22].

This paper deals with the effect of AVR gain on the bifurcations of SSR in power systems. The first system of the IEEE second benchmark model of SSR is chosen for the numerical investigation. The bifurcation parameter is the compensation factor, which is the ratio between the reactance of the series capacitor and that of the inductor of the compensated transmission line. The dynamics of the *d*- and *q*-axes damper windings and PSS are included. The variation of the Hopf bifurcation location as function of the AVR gain for two operation conditions is obtained. Some time domain simulations based on the nonlinear dynamical model are carried out at different compensation factors and AVR gains. The paper is organized as follows. Section 2 briefly summarizes some of the bifurcation theory. Section 3 presents the system under study together with its complete nonlinear dynamical mathematical model. The numerical simulation results and the time domain simulations are given in Section 4. Finally, conclusions are drawn in Section 5.

2. Bifurcation theory [23]

Bifurcation is a qualitative and/or quantitative change in the behavior of a nonlinear system when one or more of its parameters change. For example, the stability of an equilibrium solution changes from locally asymptotically stable to unstable at certain values of the system parameters. These changes are called bifurcations and the parameter values at which the changes occur are called bifurcation values. Hopf bifurcation addresses local bifurcations in a family of differential equations, which depends on a scalar parameter and an isolated equilibrium that has a unique pair of complex conjugate eigenvalues with zero real part at a certain bifurcation parameter value.

Consider the following nonlinear dynamical autonomous system:

$$\frac{dx}{dt} = F(x;\mu) \tag{1}$$

where μ is the bifurcation parameter. The equilibrium solutions are obtained by dropping out all the time derivative terms and solving the resulted nonlinear set of algebraic equations:

$$F(x;\mu) = 0 \tag{2}$$

Let the solution for $\mu = \mu_o$ be x_o. To determine the stability of this equilibrium solution, a small disturbance y is superimposed on it i.e.

$$x(t) = x_o + y(t) \tag{3}$$

Substituting Eq. (3) into Eq. (1) yields:

$$\frac{dy}{dt} = F(x_o + y;\mu_o) \tag{4}$$

Expanding Eq. (4) in a Taylor series about x_o, and retaining only linear terms in the disturbance leads to

$$\frac{dy}{dt} = F(x_o;\mu_o) + D_x F(x_o;\mu_o)y + O(|y|^2) \tag{5}$$

or

$$\frac{dy}{dt} \approx D_x F(x_o;\mu_o)y = Ay \tag{6}$$

where A is the matrix of the first partial derivatives defined at the operating point. It is called the Jacobean matrix. The eigenvalues of this constant matrix provides information about the local stability of the equilibrium solution x_o. It is said local because a small disturbance and linearizing the vector field is considered. If all of the eigenvalues of A have negative real parts, then all of the

components of the disturbance y decay in time, and hence x approaches the equilibrium x_o as $t \to \infty$. Therefore, the equilibrium solution x_o is asymptotically stable.

A Hopf bifurcation of an equilibrium solution occurs if the following conditions are satisfied:

1. $F(x_o;\ \mu_o) = 0$.
2. The matrix A has a pair of purely imaginary eigenvalues $\pm i\omega_h$, while the other eigenvalues have nonzero real parts at $(x_o;\ \mu_o)$.
3. For $\mu \approx \mu_o$, let the analytical continuation of the pair imaginary eigenvalues be $\hat{\lambda} \pm i\omega$. Then $(d\hat{\lambda}/d\mu) \neq 0$ at $\mu = \mu_0$. This condition implies a transversal or nonzero speed crossing of the imaginary axis and hence is called the transversality condition.

Unlike equilibrium solutions, periodic solutions are characterized by time-varying states. A periodic solution is a dynamic solution that is characterized by one basic frequency. The spectrum of a periodic signal consists of spike at the base frequency and spikes at integer multiples of the base frequency. The amplitude of some of these frequencies may be zero. A solution $x = X(t)$ of a continuous-time system is periodic with least period T if $X(t + T) = x(T)$ and $X(t + \tau) \neq x(t)$ for $0 < \tau < T$. A periodic solution is called a limit cycle if there are no other periodic solution sufficiently close to it. In other words, a limit cycle is an isolated periodic solution and corresponds to an isolated closed orbit in the state space. Every trajectory initiated near a limit cycle approaches it either as $t \to \infty$ or as $t \to -\infty$.

Generally, the situation in the case of a Hopf bifurcation can be further classified according to whether the bifurcation is subcritical or supercritical. To describe these possibilities further, let the critical parameter value be μ_c and suppose that $x_o(\mu)$ is stable for $\mu < \mu_c$ but unstable for $\mu > \mu_c$. In subcritical Hopf bifurcation, unstable periodic orbits of small amplitude emerge from $x_o(\mu_c)$ and exist locally for $\mu < \mu_c$. In the supercritical Hopf bifurcation, a stable periodic orbit emerges at μ_c and exists for $\mu > \mu_c$. In the subcritical case, an initial condition near $x_o(\mu)$ for $\mu > \mu_c$ will tend to diverge away from the nominal equilibrium. In contrast, for a supercritical Hopf bifurcation, the same initial condition would result in an oscillatory motion in the immediate vicinity of x_o. therefore, the supercritical bifurcation results in a more desirable system response than the subcritical bifurcation, locally near $\mu = \mu_c$.

3. System description and mathematical model

The considered system is the first system of the IEEE second benchmark model of SSR. It is a SMIB power system with two transmission lines, one of them is compensated by series capacitor as shown in Fig. 1, [24].

The mechanical mass–spring–damper system corresponding to the electrical system is shown in Fig. 2. It consists of exciter (Ex.), generator (Gen.), low-pressure (LP) and high-pressure (HP) turbine sections. Every section has its own angular momentum constant M and damping coefficient D, also every two successive masses have their own shaft stiffness constant K.

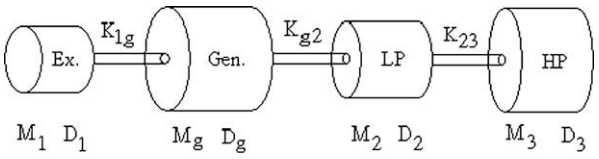

Fig. 2. Mechanical mass–spring–damper system.

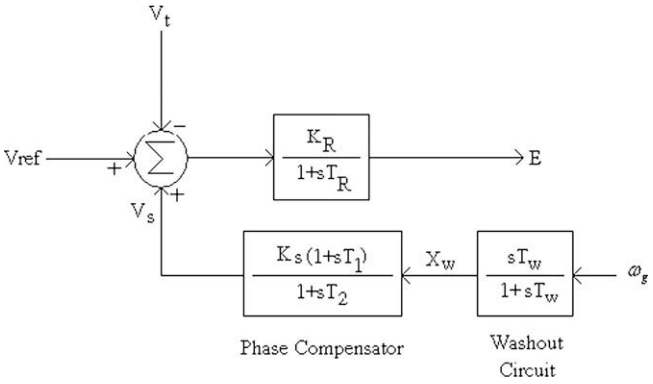

Fig. 3. Block diagram of the AVR and PSS.

The block diagram of AVR and PSS is shown in Fig. 3. The AVR consists of one time constant T_R and gain K_R. The PSS consists of washout circuit and phase compensator. The numerical parameters of the complete electro-mechanical system are given in Appendix A.

The mathematical model of the synchronous generator, transmission line, mechanical system, AVR and PSS can be summarized as [25] follows.

3.1. Synchronous generator

The stator of the synchronous generator consists of three-phase winding, the rotor consists of field and damper windings. The field winding is connected to a source of direct current while the damper windings are short-circuited and only one damper winding is assumed in each axis. Applying Park's transformation yields the following five equations corresponding to each winding:

$$X_{ffd}\frac{di_{fd}}{dt} - X_{afd}\frac{di_d}{dt} + X_{fkd}\frac{di_{kd}}{dt} = \omega_o \frac{r_{fd}}{X_{afd}}E - \omega_o r_{fd} i_{fd} \tag{7}$$

$$\begin{aligned} X_{afd}\frac{di_{fd}}{dt} - (X_d + X_T + kX_{L1} + X_b)\frac{di_d}{dt} + X_{akd}\frac{di_{kd}}{dt} \\ = \omega_o V_o \sin\delta_g + \omega_o(R_b + R_T + kR_1 + r_a)i_d \\ - \omega_o(X_T + X_b + kX_{L1} + \omega_g X_q)i_q + \omega_o \omega_g X_{akq} i_{kq} + \omega_o v_{cd} \end{aligned} \tag{8}$$

where $k = \frac{\sqrt{R_2^2 + X_{L2}^2}}{\sqrt{(R_1+R_2)^2 + (X_{L1}+X_{L2}-\mu X_{L1})^2}}$ and $\mu = \frac{X_c}{X_{L1}}$; the compensation factor.

$$X_{fkd}\frac{di_{fd}}{dt} - X_{akd}\frac{di_d}{dt} + X_{kkd}\frac{di_{kd}}{dt} = -\omega_o r_{kd} i_{kd} \tag{9}$$

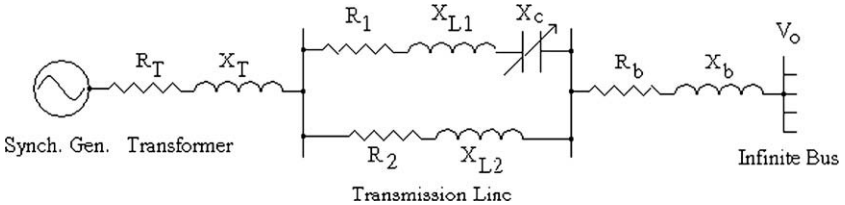

Fig. 1. Electrical system under study (system 1, IEEE second benchmark model of SSR).

$$-(X_q + X_T + kX_{L1} + X_b)\frac{di_q}{dt} + X_{akq}\frac{di_{kq}}{dt} = \omega_o V_o \cos\delta_g - \omega_o\omega_g X_{afd} i_{fd} + \omega_o(X_T + X_b + kX_{L1} + \omega_g X_d) i_d - \omega_o\omega_g - X_{akd} i_{kd} + \omega_o(R_T + R_b + kR_1 + r_a) i_q + \omega_o v_{cq} \quad (10)$$

$$-X_{akq}\frac{di_q}{dt} + X_{kkq}\frac{di_{kq}}{dt} = -\omega_o r_{kq} i_{kq} \quad (11)$$

3.2. Transmission line

$$\frac{dv_{cd}}{dt} = \omega_o k\mu X_{L1} i_d + \omega_o v_{cq} \quad (12)$$

$$\frac{dv_{cq}}{dt} = \omega_o k\mu X_{L1} i_q - \omega_o v_{cd} \quad (13)$$

3.3. Mechanical system

$$\frac{d\delta_1}{dt} = \omega_o\omega_1 - \omega_o \quad (14)$$

$$M_1\frac{d\omega_1}{dt} = D_1 - D_1\omega_1 - K_{1g}\delta_1 + K_{1g}\delta_g \quad (15)$$

$$\frac{d\delta_g}{dt} = \omega_o\omega_g - \omega_o \quad (16)$$

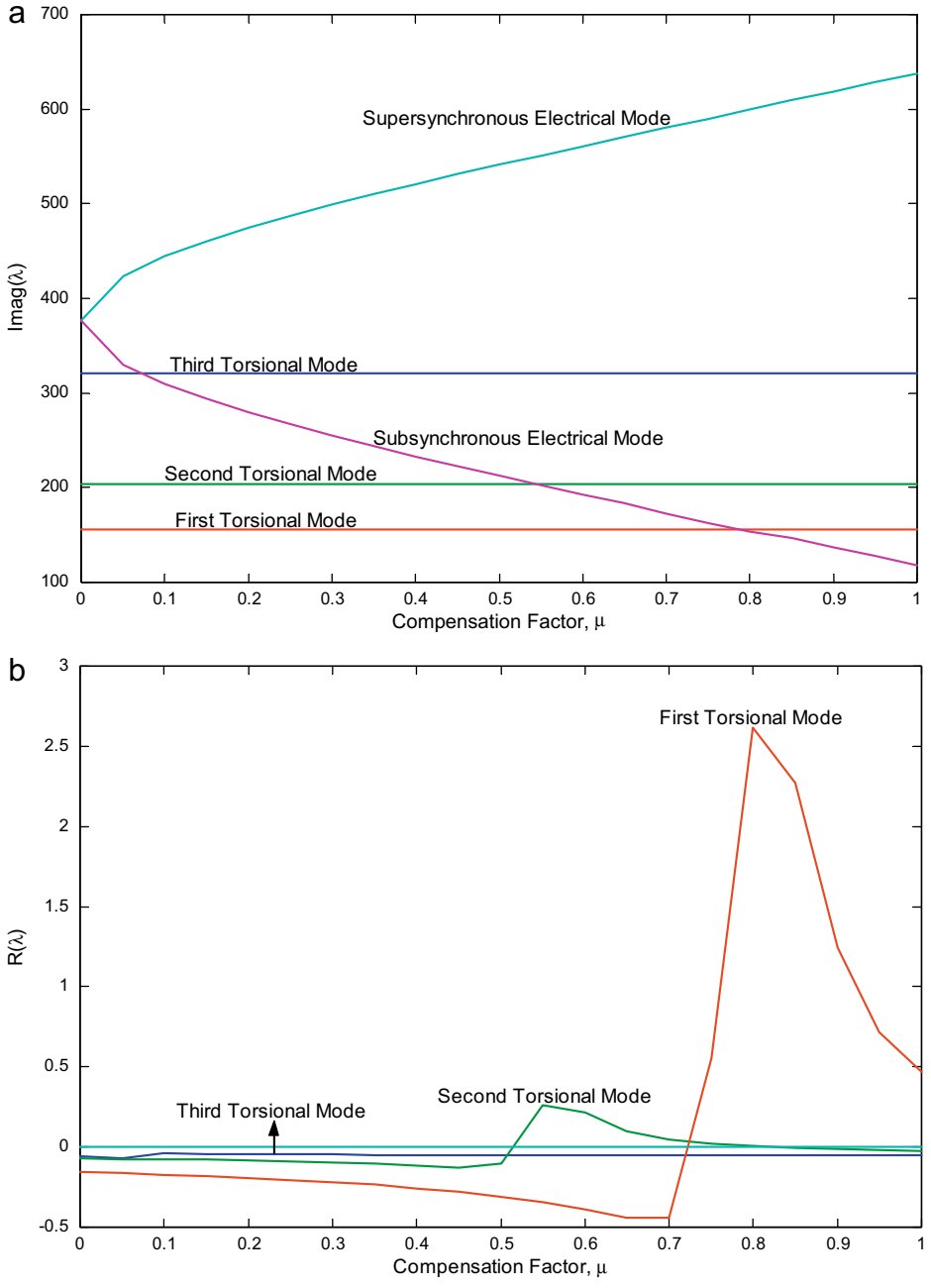

Fig. 4. Variation of (a) imaginary (b) real parts of eigenvalues of the linearized model around the operating point as function of the compensation factor μ with $K_R = 100$.

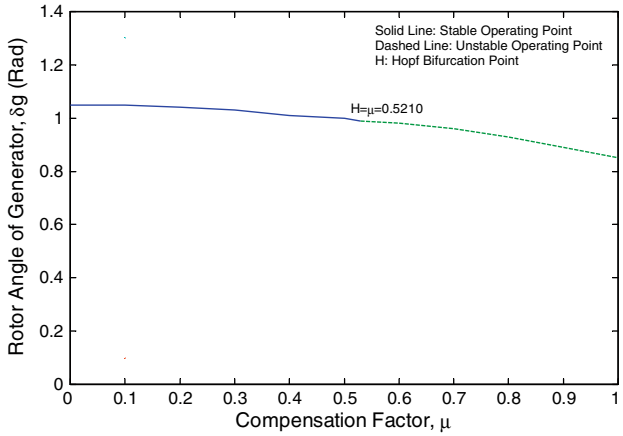

Fig. 5. Bifurcation diagram with $K_R = 100$, rotor angle of generator δ_g as function of the compensation factor μ.

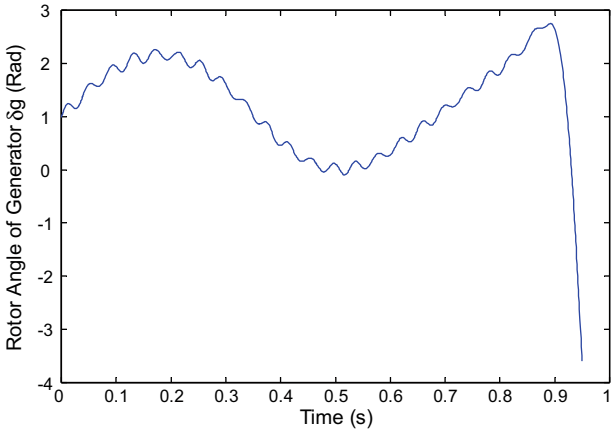

Fig. 6. Rotor angle of generator δ_g after 9% initial disturbance on the speed of the generator at $\mu = 0.515$ (slightly before the Hopf bifurcation point).

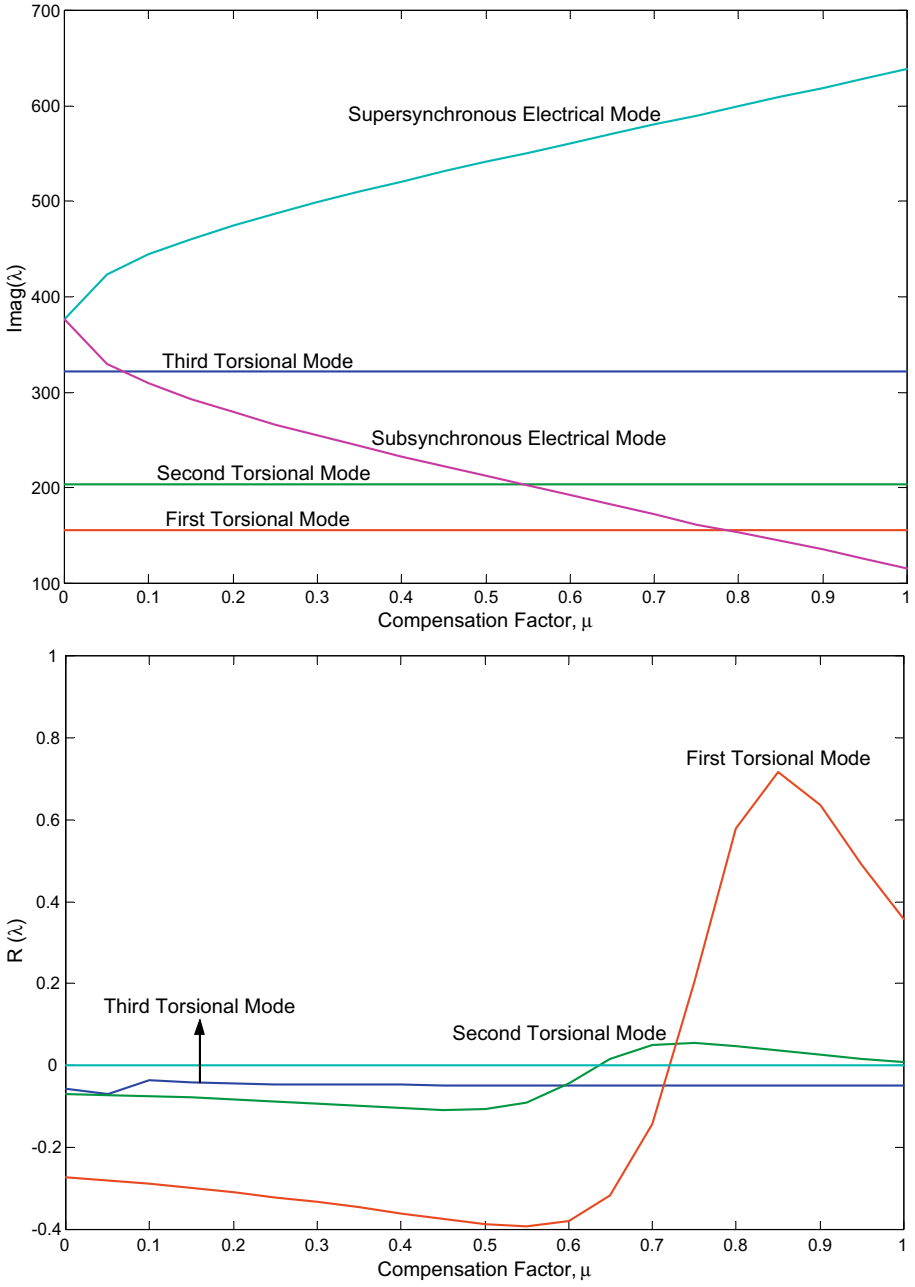

Fig. 7. Variation of (a) imaginary (b) real parts of eigenvalues of the linearized model around the operating point as function of the compensation factor μ with $K_R = 1000$.

$$M_g\frac{d\omega_g}{dt} = T_m + D_g - X_{afd}i_q i_{fd} + X_d i_q i_d - X_{akd}i_{kd}i_q - X_q i_q i_d + X_{akq}i_{kq}i_d - D_g\omega_g + K_{1g}\delta_1 - K_{1g}\delta_g - K_{g2}\delta_g + K_{g2}\delta_2 \quad (17)$$

$$\frac{d\delta_2}{dt} = \omega_o\omega_2 - \omega_o \quad (18)$$

$$M_2\frac{d\omega_2}{dt} = D_2 - D_2\omega_2 + K_{g2}\delta_g - K_{g2}\delta_2 - K_{23}\delta_2 + K_{23}\delta_3 \quad (19)$$

$$\frac{d\delta_3}{dt} = \omega_o\omega_3 - \omega_o \quad (20)$$

$$M_3\frac{d\omega_3}{dt} = D_3 - D_3\omega_3 + K_{23}\delta_2 - K_{23}\delta_3 \quad (21)$$

3.4. AVR and PSS

$$T_W\frac{dX_W}{dt} - T_W\frac{d\omega_g}{dt} = -X_W \quad (22)$$

$$T_2\frac{dV_s}{dt} - T_1K_s\frac{dX_W}{dt} = K_sX_W - V_s \quad (23)$$

$$T_R\frac{dE}{dt} = K_RV_{ref} + K_RV_s - K_RV_t - E \quad (24)$$

where $V_t = \sqrt{V_d^2 + V_q^2}$, neglecting stator transients yields:

$$V_t = \sqrt{(-r_a i_d + X_q i_q)^2 + (-r_a i_d - X_d i_d + X_{afd}i_{fd})^2}$$

4. Numerical simulations

This section presents the bifurcation analysis and some time domain simulations with different AVR gains. The bifurcation parameter is the compensation factor, which is the ratio between the reactance of the series capacitor and that of the inductor. Particularly, as the compensation factor increases, the power transfer capability of the transmission line increases. However, the operating point of the system may not keep its stability at some compensation factors. Therefore, the operating point stability regions must be studied at all realistic compensation factors. The variation of the imaginary and real parts of the prime interest eigenvalues of the linearized model around the operating point with K_R = 100 as function of the compensation factor is shown in Fig. 4. As the compensation factor increases, the supersynchronous electrical mode increases while that of the subsynchronous decreases and interacts successively with the third, second and first torsional mechanical modes at $\mu \approx 0.0723$, 0.5455 and 0.7922, respectively. Fortunately, the first interaction was not strong enough to make any change in the stability of the operating point of the system. However, the second interaction was able to transversally move the corresponding real parts of the eignevalues from left- to the right-half of the complex plane at $\mu \approx 0.5210$. Therefore, a Hopf bifurcation took place. The second torsional mode regains its stability in a reverse Hopf bifurcation at $\mu \approx 0.8225$. However, the operating point of the system didn't regain its overall stability as the first torsional mode had previously lost it at $\mu \approx 0.7223$ as a result of the strongest interaction with the first torsional mode. The equilibrium stability regions are shown in the bifurcation diagram of Fig. 5 in δ_g–μ plane. The power system has a stable operating point in the region $0 < \mu < 0.5210$, unstable operating point in the region $0.5210 < \mu < 1$ and a Hopf bifurcation point at $\mu = H \approx 0.5210$.

Now we reached a point at which we should determine the type of the dynamic bifurcation i.e. subcritical or supercritical Hopf bifurcation. Fig. 6 shows the response of the system (rotor angle of generator δ_g) after a 9% initial disturbance on the speed of the generator at $\mu = 0.515$, (slightly before the Hopf bifurcation point

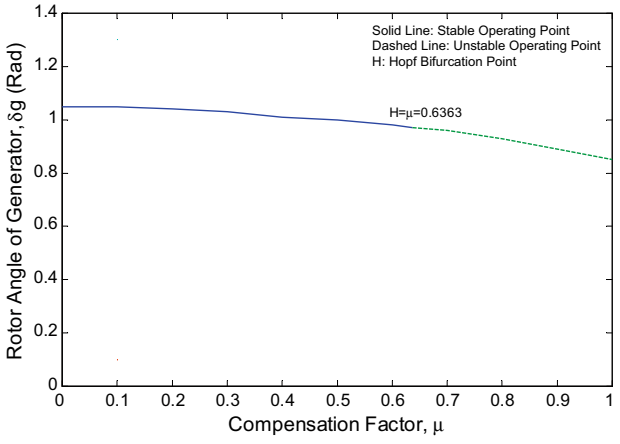

Fig. 8. Bifurcation diagram with K_R = 1000, rotor angle of generator δ_g as function of the compensation factor μ.

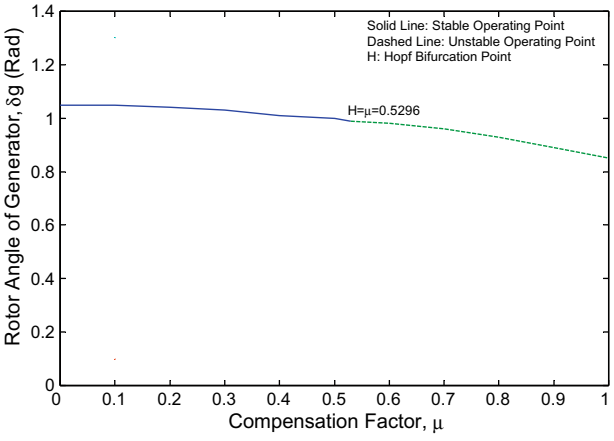

Fig. 9. Bifurcation diagram with K_R = 2000, rotor angle of generator δ_g as function of the compensation factor μ.

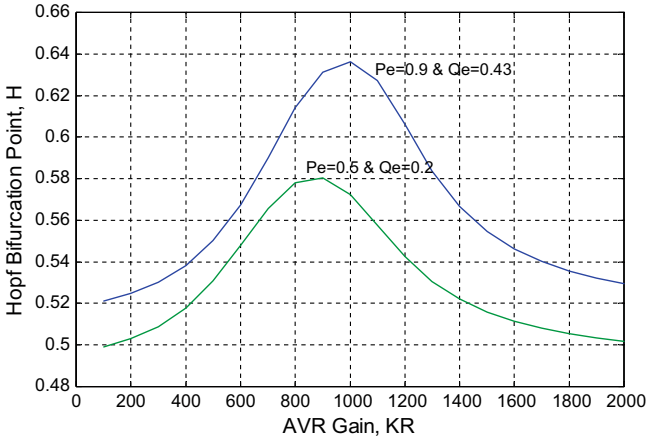

Fig. 10. Hopf bifurcation point as function of AVR gain K_R for two operating points.

$H \approx \mu = 0.5210$). Clearly, the system routes to unpredictable solution which indicates that the Hopf bifurcation is of subcritical type.

The operating point bifurcations of the system with K_R equals 1000 is repeated. Fig. 7 shows the variation of the imaginary and real parts of the prime interest eigenvalues of the linearized model around the operating point. In this case, the moving of the real parts of the second torsional mode from left- to right-half of the complex plane as a result of the interaction of the subsynchronous electrical mode with the second torsional mode has been delayed. The Hopf bifurcation occurred at $\mu = H \approx 0.6363$ (it was at $\mu = 0.5210$ in the previous case when $K_R = 100$). The bifurcation diagram for this case, the rotor angle of generator δ_g against the compensation factor μ, is shown in Fig. 8. The operating point is stable in the range $0 < \mu < 0.6363$, unstable in the range $0.6363 < \mu < 1$ and has a Hopf bifurcation point at $\mu = H \approx 0.6363$.

The study of the operating point bifurcation is repeated for an AVR gain $K_R = 2000$. Now, the Hopf bifurcation took place at a compensation factor $\mu = H \approx 0.5296$ (it was at $\mu = 0.5210$ in case of $K_R = 100$ and $\mu = 0.6363$ in case of $K_R = 1000$). The bifurcation diagram for this case is shown in Fig. 9. The system has a stable operating point in the range $0 < \mu < 0.5296$, unstable operating point in the range $0.5296 < \mu < 1$ and a Hopf bifurcation point at $\mu = H \approx 0.5296$.

From the previous discussions, it is obvious that the AVR gain affects the location of the Hopf bifurcation point of the system.

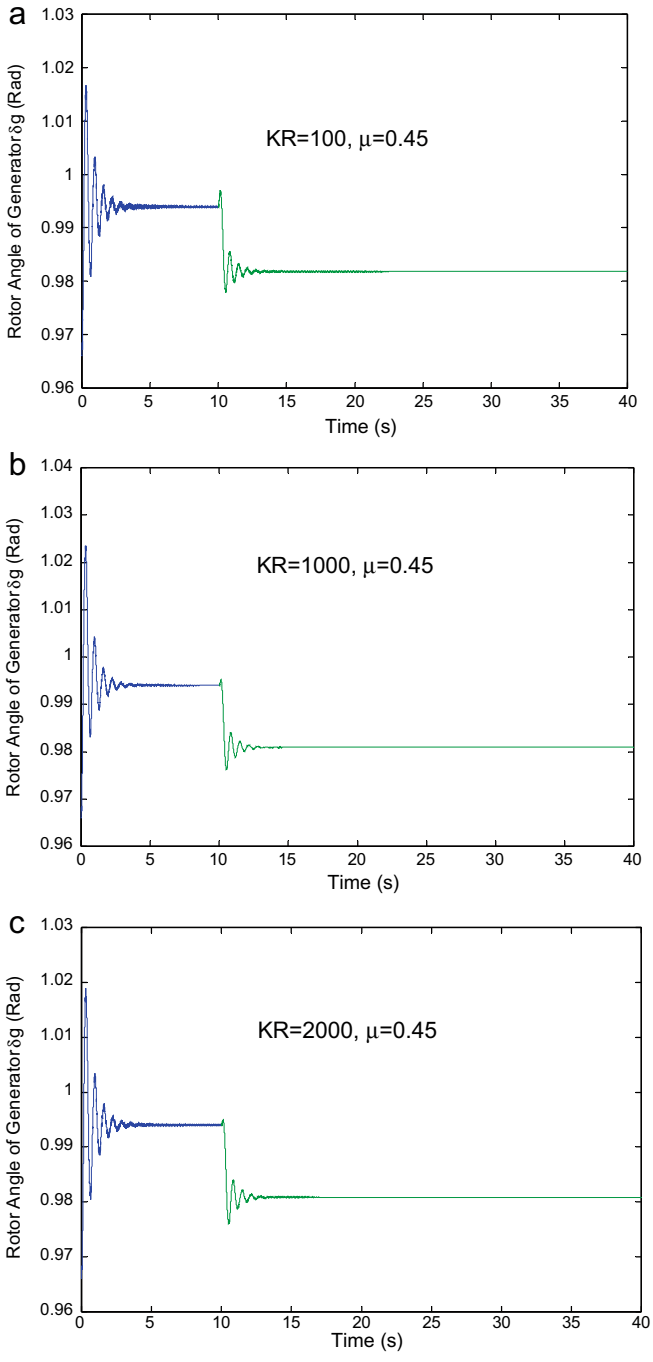

Fig. 11. Rotor angle of generator δ_g response at $\mu = 0.45$ after a 0.02 pu step decrease in the infinite bus voltage with (a) $K_R = 100$, (b) $K_R = 1000$, and (c) $K_R = 2000$.

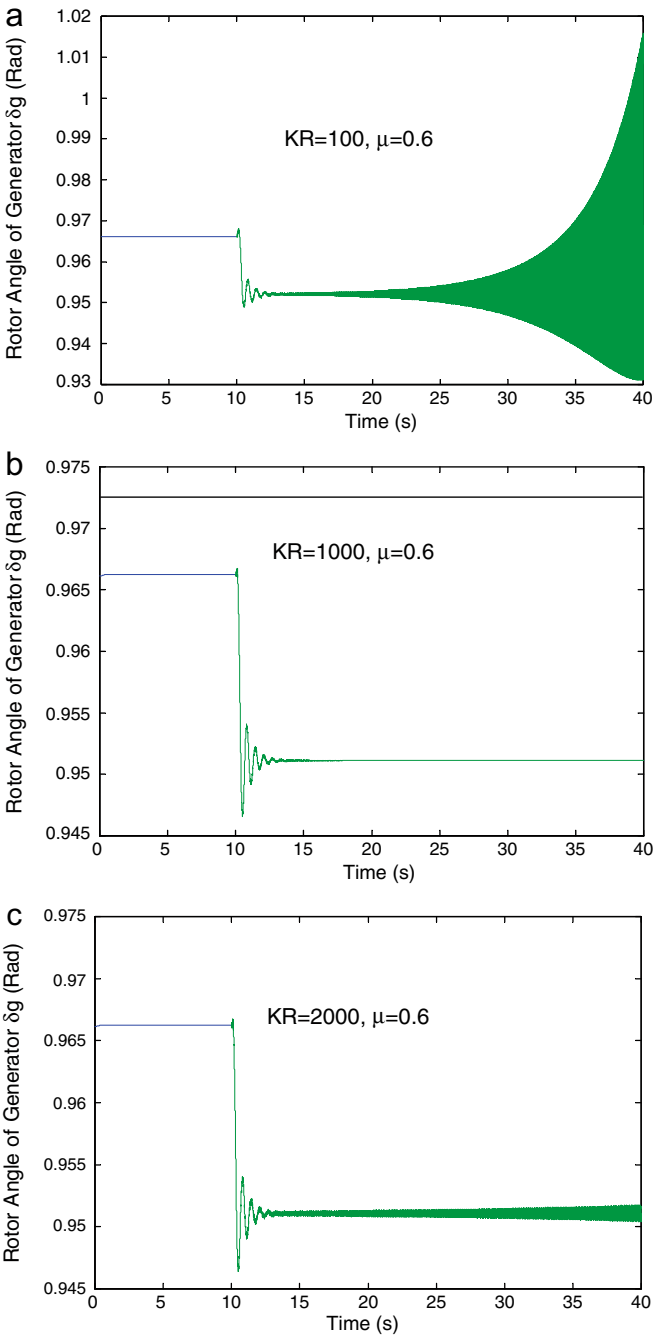

Fig. 12. Rotor angle of generator δ_g at $\mu = 0.6$ after a 0.02 pu step decrease in the infinite bus voltage with (a) $K_R = 100$, (b) $K_R = 1000$, and (c) $K_R = 2000$.

The variation of the Hopf bifurcation point as function of the AVR gain is shown in Fig. 10. As the AVR gain increases, the Hopf bifurcation point increases up to a gain of about 1000 in case of heavily loaded machine with $P_e = 0.9$ pu and $Q_e = 0.43$ pu. An AVR gain of about 900 provides the biggest stable region in case of $P_e = 0.5$ pu and $Q_e = 0.2$ pu. In both cases, the location of the Hopf bifurcation point starts decreasing when AVR gain passes beyond this value. Therefore, for this system an AVR gain in the range of 1000 is the best from the operating point stability region point of view.

Time domain simulations for the system have been carried out based on the nonlinear dynamical mathematical model with different compensation levels and AVR gains. Fig. 11a–c shows the response of the system after a 0.02 pu step decrease on the infinite bus voltage applied at $t = 10$ s at a compensation factor of 0.45 with AVR gains of 100, 1000 and 2000, respectively. The operating point of the system is stable in all cases. The response of the system after the same disturbance at a compensation factor of 0.6 with the same AVR gains is shown in Fig. 12a–c. The operating point of the system is stable only when the AVR gain is 1000 (the Hopf bifurcation point was at $\mu = H \approx 0.6363$). These results coincide with that obtained from the operating point bifurcation analysis.

5. Conclusions

The effect of AVR gain on the bifurcations of the first system of the IEEE second benchmark model of SSR is studied. The dynamics of the two axes damper windings and PSS are included. In all cases, the operating point of the system losses stability via Hopf bifurcation as a pair of complex conjugate eigenvalues of the linearized model around the operating point transversally crosses from left- to right-half of the complex plan. It is found that this Hopf bifurcation is of subcritical type. The results show that the AVR gain affects the location of the Hopf bifurcation point. For this system, an AVR gain in the range of 1000 provides the best bifurcation point location. Time domain simulations based on the nonlinear dynamical mathematical model after step decrease in the infinite bus voltage are carried out at different AVR gains and compensation levels. They coincide with the results of the bifurcation analysis.

Appendix A

The numerical parameters of the synchronous generator, transmission line, mechanical system, AVR and PSS are:

A.1. Synchronous generator (in pu on the base of its ratings)

$X_{ffd} = 1.6286$, $X_{afd} = 1.5100$, $X_{fkd} = 1.5100$, $r_{fd} = 0.00096$, $X_d = 1.6500$, $X_{akd} = 1.5100$, $r_a = 0.0045$, $X_q = 1.5900$, $r_{kd} = 0.0160$, $X_{akq} = 1.4500$, $X_{kkd} = 1.6420$, $X_{kkq} = 1.5238$, $r_{kq} = 0.0116$.

A.2. Transmission line (in pu on the base of generator ratings)

$X_T = 0.1200$, $X_{L1} = 0.4800$, $X_b = 0.1800$, $R_b = 0.0084$, $R_T = 0.0012$, $R_1 = 0.0444$, $R_2 = 0.0402$, $X_{L2} = 0.4434$.

A.3. Mechanical system (in pu on the base of the generator ratings)

$M_1 = 0.0138$, $D_1 = 1.5100$, $K_{1g} = 3.7363$, $M_g = 1.7581$, $D_g = 0.1758$, $K_{g2} = 83.3823$, $M_2 = 3.1004$, $D_2 = 0.3100$, $K_{23} = 42.6572$, $M_3 = 0.4980$, $D_3 = 0.0498$.

A.4. AVR and PSS

$K_R = 100-2000$, $T_R = 0.025$s, $T_W = 10$s, $K_s = 2$, $T_1 = 0.048$s, $T_2 = 0.032$s.

References

[1] Padiyar KR. Analysis of subsynchronous resonance in power systems. Kluwer Academic Publisher; 1999.
[2] Fouad AA, Khu KT. Subsynchronous resonance zones in the IEEE bench mark power system. IEEE Trans PAS 1978;PAS-97(15):754–62.
[3] Yan A, Yu Y. Multi-mode stabilization of torsional oscillations using output feedback excitation control. IEEE Trans PAS 1982;PAS-101:1245–53.
[4] Iravani MR, Edris AA. Eigen analysis of series compensation schemes reducing the potential of subsynchronous resonance. IEEE Power System Summer Meeting; 1994.
[5] Framer RG, Katz E, Schwalb AL. Navajo project on subsynchronous resonance analysis and solutions. IEEE Trans PAS 1985:1057–66.
[6] Edris A. Series compensation schemes reducing the potential of resonance. IEEE Trans PAS 1990:219–26.
[7] Rana RD, Huff SW, Hayes RM, Fromholtz EN, Schulz RP. AEP's Kanawha river 345kV series capacitor installations-subsynchronous resonance studies and torsional measurements. In: Proceedings of the American power conference; 1991, p. 300–5.
[8] Zhu W, Spee R, Mohler RR, Alexander GG, Mittelstadt WA, Maratuhulam D. An EMTP study of SSR mitigation using the thyristor controlled series capacitor. IEEE Trans Power Delivery 1995;10:1479–85.
[9] Dobson I, Chiang HD. Towards a theory of voltage collapse in electric power systems. Syst Cont lett 1989;13:253–62.
[10] Ajjarapu A, Lee B. Bifurcation theory and its applications to nonlinear dynamical phenomena in an electrical power system. IEEE Trans Power Syst 1992;7(1):424–31.
[11] Nayfeh AH, Harb AM, Chin Char-Ming. Bifurcations in a power system model. Int J Bifurcat Chaos 1996;6(3):497–512.
[12] Rajesh KG, Padiyar KR. Bifurcation analysis of a three node power system with detailed models. Elect Power Energy Syst 1999;21:375–93.
[13] Nayfeh AH, Harb AM, Chin Char-Ming, Hamdan AMA, Mili Lamine. Applications of bifurcation theory to subsynchronous resonance in power systems. Int J Bifurcation and Chaos 1998;8(1):157–72.
[14] Harb AM, Milli L, Nayfeh AH, Chin C-M. On the effect of the machine saturation on SSR in power systems. Elect Machines Power Syst 2000;28:1019–35.
[15] Wang OH, Abed EH. Bifurcation control of chaotic systems. Automatica 1995;31:1213–26.
[16] Chen G, Dong X. From chaos to order: methodologies, perspectives and applications. Singapore: World Scientific; 1998.
[17] Berns DW, Moiola JL, Chen G. Feedback control of limit cycle amplitude from a frequency domain approach. Automatica 1998;34:1567–73.
[18] Basso M, Evangelisti A, Genesio R, Tesi A. On bifurcation control in time delay feedback systems. Int J Bifurcat Chaos 1998;8:713–21.
[19] Ahmad M. Harb, Application of Bifurcation theory to subsynchronous resonance in power systems. PhD thesis, Virginia Polytechnic Institute and State University, USA, 1996.
[20] Harb AM, Widyan MS. Chaos and bifurcation control of SSR in the IEEE second benchmark model. Chaos Solitons Fractals J 2004;21:537–52.
[21] Harb AM, Widyan MS. Controlling chaos and bifurcation of subsynchronous resonance in power systems. Nonlinear anal Model Control J 2002;7(2):15–36.
[22] A.M. Harb, M.S. Widyan, Modern nonlinear theory as applied to ssr of the IEEE second benchmark model. In: IEEE Bologna power tech 2003 conference, June 23–26, 2003, Bologna, Italy.
[23] Nayfeh AH, Balachandran B. Applied nonlinear dynamics. New York: John Wiley; 1995.
[24] IEEE Subsynchronous Resonance Working Group. Second benchmark model for computer simulation of subsynchronous resonance. IEEE Trans PAS 1985;PAS-104(6).
[25] Yu Y. Electric power system dynamics. New York: Academic Press; 1993.